Appl Phys B (2012) 107:1175–1180
DOI 10.1007/s00340-011-4870-z

Applied Physics B
Lasers and Optics

Background-free detection of trapped ions

N.M. Linke · D.T.C. Allcock · D.J. Szwer · C.J. Ballance · T.P. Harty · H.A. Janacek · D.N. Stacey · A.M. Steane · D.M. Lucas

Received: 10 June 2011 / Revised version: 30 August 2011 / Published online: 14 January 2012

Abstract We demonstrate a Doppler cooling and detection scheme for ions with low-lying D levels which almost entirely suppresses scattered laser light background, while retaining a high fluorescence signal and efficient cooling. We cool a single ion with a laser on the $^2S_{1/2} \leftrightarrow {}^2P_{1/2}$ transition as usual, but repump via the $^2P_{3/2}$ level. By filtering out light on the cooling transition and detecting only the fluorescence from the $^2P_{3/2} \rightarrow {}^2S_{1/2}$ decays, we suppress the scattered laser light background count rate to 1 s^{-1} while maintaining a signal of 29000 s^{-1} with moderate saturation of the cooling transition. This scheme will be particularly useful for experiments where ions are trapped in close proximity to surfaces, such as the trap electrodes in microfabricated ion traps, which leads to high background scatter from the cooling beam.

1 Introduction

In recent years trapped ions have been at the heart of an increasing range of experiments and proposals [1, 2], most prominently the field of quantum information processing (QIP). There has been a significant trend towards ever-smaller two- and three-dimensional trap geometries, as well as towards integration of imaging optics [3] and optical cavities [4–7] with the trap electrode structure. There have also been studies of trapped ions' interactions with a thin conducting wire [8] and proposals to extend this to a nanofibers [9] in order to couple ions to the fiber's evanescent light field (as previously implemented with neutral atoms [10, 11]). Other experiments pursue the entanglement of the internal state of a trapped ion with the vibrational mode of a cantilever in order to study quantum effects in meso- and macroscopic objects [12].

Many of these experiments rely on ions being trapped close to surfaces and all of them depend on laser cooling [13] as the standard technique to reduce the ions' motion. For its large velocity capture range, high cooling rates and straightforward implementation, Doppler cooling is usually the initial stage of the cooling process [14]. In a two-level approximation the Doppler cooling limit temperature $T = \hbar\Gamma/2k_B$ (where Γ is the natural line width of the cooling transition) is achieved in the limit of low laser intensity. However, the cooling rate is greater at higher intensities, where the photon scattering rate is larger, and in practice intensities around the saturation intensity $I_{sat} = 2\pi hc\Gamma/\lambda^3$ (where λ is the transition wavelength) offer a good compromise between these competing demands. Maintaining a high cooling efficiency is particularly important in surface-electrode ion traps, where the shallower trap depth can lead to ion loss after background gas collisions if the cooling rate is low and where anomalous heating effects are more prevalent than in three-dimensional traps due to the proximity of the ion to the trap electrodes.

When detecting a fluorescence signal S from ions trapped in close proximity on the order of 100 μm or less to surfaces (the trap electrodes, integrated optics or other objects of study), light scattered off the surroundings is picked up by the imaging or detection optics and can significantly increase the background signal B. The signal is usually shot-noise limited, so the signal-to-noise ratio is given by

N.M. Linke · D.T.C. Allcock · D.J. Szwer · C.J. Ballance · T.P. Harty · H.A. Janacek · D.N. Stacey · A.M. Steane · D.M. Lucas (✉)
Department of Physics, University of Oxford, Parks Road, Oxford OX1 3PU, UK
e-mail: d.lucas@physics.ox.ac.uk

Present address:
D.J. Szwer
Department of Physics, University of Durham, Durham, UK

$S/\sqrt{S+B}$ and reducing the background is clearly advantageous (see [15] for a more detailed discussion of discrimination of single-ion fluorescence from background). Previous work achieved negligible background by driving the narrow dipole-forbidden $S_{1/2} \leftrightarrow D_{5/2}$ transition in $^{40}Ca^{+}$ with ∼250 mW of laser intensity and collecting fluorescence on allowed decay transitions [16]; however, this had the disadvantages of reducing both the cooling and fluorescence rates significantly, and requiring a more complex laser system.

Here, we describe a new scheme that achieves detection at essentially zero background but only uses dipole-allowed transitions and hence does not require a high-power or narrow-line-width laser. After a brief outline of the experimental setup, we describe four different repumping schemes for $^{40}Ca^{+}$ (which are readily applicable to ions with similar level structure), implement them and compare the results. A similar method has previously been used in magneto-optical trapping of neutral ^{85}Rb [17].

We note that the new repumping schemes introduced here, whilst useful for detecting the ion itself, are not applicable to detection of the internal state of the ion by the electron-shelving technique [18] because the $D_{5/2}$ 'shelf' is part of the cooling cycle. However, they could be useful in the context of ion-trap QIP, for example for monitoring fluorescence and maximizing the cooling rate for sympathetic-cooling ions [19]. Since they concern photon detection, they also have no influence on the charging effects caused by scattering light off surfaces close to the ion, as described in [20].

2 Experimental setup

Figure 1 shows a sketch of the trap and detection system. Single $^{40}Ca^{+}$ ions are trapped in a linear surface-electrode radio-frequency (RF) microchip trap fabricated at Sandia National Laboratories (for details, please refer to [21] and [22]). The electrode surfaces are aluminium, supported above the silicon substrate by silicon dioxide insulating pillars, and the electrodes overhang the pillars to shield trapped ions from the insulating surfaces. The ion is trapped 84 μm above the plane of the electrodes. The radial confinement is provided by a harmonic RF pseudo-potential driven at 33 MHz with an amplitude of 200 V_{pp}, which gives a radial trap frequency of 3.2 MHz. Further electrodes carry DC potentials to provide for axial confinement (axial trap frequency 1.0 MHz), tilting of the radial principal axes and micromotion compensation. The trap is enclosed in an ultra-high-vacuum chamber with a residual pressure of $<1 \times 10^{-11}$ Torr. An ion is loaded isotope selectively by photo-ionization [23] from a beam of neutral calcium atoms provided by a thermal oven. The oven is mounted behind the trap chip, sending the atoms through a slit (width 100 μm) in the trap centre. The applied magnetic field is approximately 2.4 G and aligned perpendicular to the chip.

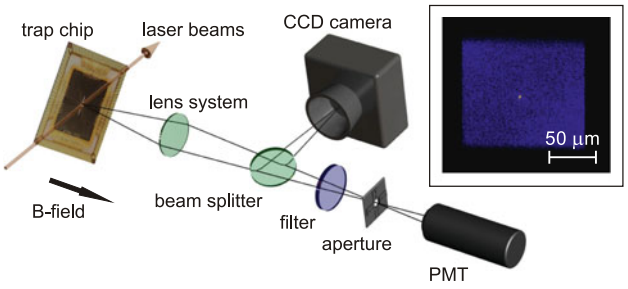

Fig. 1 Experimental setup. The ion is trapped in a surface trap, *left*. All laser beams are superimposed and propagate at 45° to the trap axis; they are linearly polarized parallel to the chip surface and perpendicular to the magnetic field ($\sigma^{\pm}$ polarization). The ion is imaged through a lens system onto an adjustable aperture and a PMT, or optionally via a beam splitter onto a CCD camera. (For the image shown, the aperture was re-imaged onto the camera to show both ion and aperture.) A significant fraction of the ion fluorescence falls outside the sharp central image; with a diffraction-limited optical system the aperture could be stopped down to reduce still further the background scattered laser light. The 393-nm filters (see text) can be placed in front of the PMT

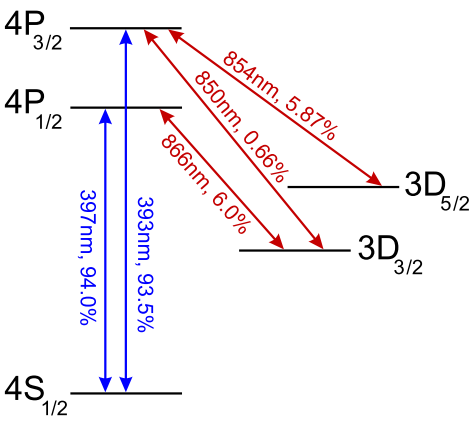

Fig. 2 Level scheme of $^{40}Ca^{+}$ with dipole transitions and their respective wavelengths and branching ratios [25]. Our repumping schemes are labeled by the number of infra-red repumpers used, prefixed by 'F' if the filter is in place and only 393-nm light is detected. A laser on the main cooling transition at 397 nm is applied in all schemes. Scheme I: 866-nm laser applied to repump, 397-nm fluorescence detected (no 393-nm light emitted). Scheme II: 850-nm and 854-nm lasers applied, both violet wavelengths detected. Scheme FII: as scheme II but only 393-nm light detected. Scheme FIII: all three infra-red lasers applied, only 393-nm light detected

Extended-cavity diode lasers at 397 nm, 850 nm, 854 nm and 866 nm are available to Doppler-cool and repump the ion (see level diagram in Fig. 2); all are locked to low-finesse optical cavities (drift rates <0.5 MHz/hour, laser line widths ≈0.5 MHz). All the laser beams are superimposed and polarized linearly perpendicular to the applied

Table 1 Experimental parameters, measured fluorescence count rates and theoretical predictions based on the optical Bloch equations. For each repumping scheme the laser powers and detunings were empirically optimized to maximize the fluorescence signal. The columns give: the optimized laser powers; whether the filters were used or not; the expected total populations of the $P_{1/2}$ and $P_{3/2}$ levels for the laser intensities used in the experiments; the predicted and measured PMT count rates (excluding background); and the measured background count rates. Agreement between the predicted and measured rates is at the 5% level (see text)

Scheme	Laser powers [μW]				Filters	Populations		Signal [counts/s]		Background [counts/s]
	397	866	850	854		$P_{1/2}$	$P_{3/2}$	Predicted	Measured	
I	22	9.9	–	–	Out	0.231	0	77102	77800	990
II	22	–	37	6.6	Out	0.357	0.022	125750	126000	990
FII	22	–	51	10	In	0.389	0.024	7651	7680	11
FIII	22	45	141	12	In	0.088	0.125	43643	41800	11

magnetic field. They are sent across the chip parallel to the surface at an angle of 45° to the trap axis. The principal axes of the pseudo-potential are tilted using a static quadrupole field (for details, see [24]) to allow cooling of all motional modes. Spot sizes ($1/e^2$ intensity radius) at the ion of the 397-nm and infra-red beams are (21 μm × 31 μm) and (17 μm × 22 μm), respectively.

The ion is observed with a photomultipler[1] (PMT) or an electron-multiplying CCD camera[2] (EMCCD) through an imaging system with a numerical aperture of 0.25 and a magnification of 8. At a focal point in the imaging path, an adjustable aperture is used to reduce background scatter. For the new repumping schemes described below, scattered laser light at 397 nm is filtered out using a pair of 393-nm interference filters[3] (with net transmission measured to be 78% and 0.3% at 393.5 nm and 397.0 nm, respectively).

3 Repumping schemes

Our Doppler cooling schemes are based on the standard $S_{1/2} \leftrightarrow P_{1/2}$ cooling transition, which in $^{40}Ca^+$ is at 397 nm (see Fig. 2). The ion has a 5% chance of decaying from the $P_{1/2}$ level into the low-lying $D_{3/2}$ level, which is long lived because the direct transition to the ground state is dipole forbidden. To repump the ion, an infra-red laser is usually applied to the $D_{3/2} \leftrightarrow P_{1/2}$ transition at 866 nm. This will be referred to as 'scheme I' here.

We can instead repump via the $P_{3/2}$ level using a laser at 850 nm. This state decays quickly to the ground state by emitting a photon at 393 nm. There is also a 5% chance of decay into the $D_{5/2}$ level from which we repump using a laser at 854 nm. This repumping technique, which we refer to as 'scheme II', makes the system into a quasi-two-level atom. It can add about 10% of 393-nm fluorescence to the signal and can increase the emitted 397-nm light by about 70%, raising the overall signal by a substantial factor (see [24] and Table 1) without increase in background.

We now consider suppression of scattered laser light background (scheme FII). Detected light at 393 nm originates exclusively from the ion which can be discriminated from the cooling light at 397 nm and all the infra-red repumping lasers. The pair of interference filters is placed in front of the PMT to block selectively the cooling light while transmitting the 393-nm light emitted by the ion. This reduces background scatter from the cooling light by more than two orders of magnitude. We then only detect the ion's fluorescence, on a background level which is dominated by the dark counts of the PMT. All the advantages of standard Doppler cooling such as the cooling rate and the velocity capture range are maintained. The overall count rate is reduced however since 397-nm light scattered by the ion is also discarded.

The detected fluorescence at 393 nm is limited by the $P_{1/2} \rightarrow D_{3/2}$ branching ratio (6.0%), since only the population decaying to $D_{3/2}$ can contribute. Scheme FIII addresses this disadvantage and achieves a higher fluorescence rate by actively pumping down more population from the $P_{1/2}$ state with the usual repumping laser at 866 nm. This increases the fluorescence rate at the cost of interconnecting several states, which creates more possibilities for two-photon dark resonances [26]. In the experimental implementation, we varied the intensities and detunings of the infra-red lasers to maximize empirically the fluorescence. The detunings are not critical because at the optimum intensities the fluorescence peak is relatively broad. We achieved a count rate within a factor of two of the standard 397 nm + 866 nm cooling scheme I.

In order to account for these experimental values, we have implemented a full optical Bloch equations model. It takes into account all Zeeman sublevels and coherence ef-

[1] Electron Tubes P25PC.

[2] Andor Luca 285_Mono, USB.

[3] Semrock FF01-387/11-25.

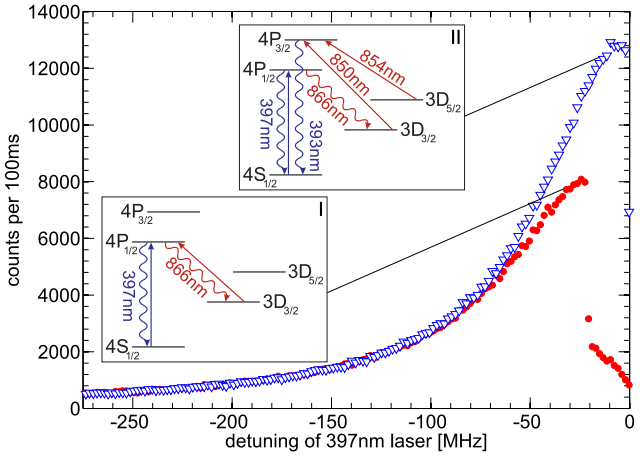

Fig. 3 PMT count rate versus detuning of the laser at 397 nm, for repumping schemes I and II. Both violet scattered wavelengths are detected. The 397-nm laser power was 22 μW. Zero detuning was inferred from the point at which the signal drops down sharply due to Doppler heating on the blue-detuned side of the resonance peak, in scheme II (in scheme I, this point occurs earlier because of a 397 nm 866 nm dark resonance). *The insets* show the two different repumping schemes. **I:** repumping with a single infra-red laser at 866 nm. **II:** repumping with two lasers at 850 nm and 854 nm

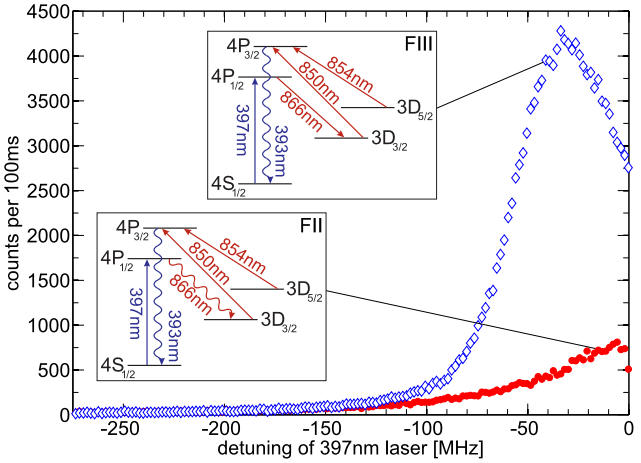

Fig. 4 PMT count rate versus detuning of the laser at 397 nm, for repumping schemes FII and FIII. The interference filters are placed in front of the PMT so that only scattered light at 393 nm is detected. The 397-nm laser power was 22 μW. *The insets* show the two different repumping schemes. **FII:** repumping with two lasers at 850 nm and 854 nm. **FIII:** repumping with all three infra-red lasers to increase the fluorescing population in $P_{3/2}$. Again, the fluorescence peaks earlier in FIII because of a 397 nm 866 nm dark resonance

fects. The $P_{1/2}$ and $P_{3/2}$ populations given by this model for our experimental parameters, and the corresponding fluorescence count rates, are compared in Table 1 for the four repumping schemes described above. When calculating the count rates from the simulated populations, the angular distribution of the fluorescence from decay of the $P_{3/2}$ level was taken into account. The agreement between the predicted and measured rates is at the 5% level. This is very satisfactory given that the empirical optimization procedure for the measured rates was only approximate. The theoretical results also depend on the direction and magnitude of the magnetic field, which are uncertain because in addition to the applied field there is an unknown ambient component. A value of $|\mathbf{B}| = 3.8$ G was chosen to give the highest level of consistency. This value is plausible given the presence of magnetic materials in the trap chip carrier, and our experience in other ion traps. For simplicity, the direction was taken to be along that of the applied field. A net detection efficiency of 0.25% at 397 nm was assumed; this is consistent both with the fluorescence spectrum in scheme I (Fig. 3) and with an independent measurement using a pulsed method [27].

It would be possible to implement a similar set of schemes by cooling on the 393-nm transition and repumping to the $P_{1/2}$ level via the 866-nm transition. Fluorescence at 397 nm could then be collected and discriminated in a similar way. However, in the limit of full saturation of all transitions only the two states in $P_{1/2}$ contribute to the fluorescence, compared with the four $P_{3/2}$ states in our scheme, leading to a lower signal.

4 Experimental implementation

In Fig. 3 fluorescence spectra from a single ion are shown for schemes I and II. No filters were placed in front of the PMT, so both violet wavelengths can contribute to the signal. The maximum signals above background are 77800 s^{-1} and 126000 s^{-1}, respectively.

Placing the band-pass filters in front of the detector cuts out almost all light at 397 nm and we only detect 393-nm fluorescence. The results of implementing schemes FII and FIII are presented in Fig. 4. The maximum signals are 7680 s^{-1} and 41800 s^{-1} respectively. Scheme FIII thus achieves a signal which is only a factor of two smaller than scheme I, but with the background reduced by two orders of magnitude.

We repeated the four experiments presented in Figs. 3 and 4 for a range of different 397-nm laser powers. At each power we took a data set with all infra-red beams turned off to determine the background, which is shown in Fig. 5a. The background is made up of the sum of the constant detector dark count rate and the rate of scatter, which is proportional to the laser power. Without the filters the background rises steeply with increasing 397-nm power (slope 44.4(6) $s^{-1}/\mu W$), while with the filters it is almost constant with a slope of only 0.16(2) $s^{-1}/\mu W$. Straight lines are fitted to the two data sets to use as smooth background data for the signal-to-background comparison. The intercepts are 7(1) s^{-1} and 6.6(4) s^{-1}, which correspond to the PMT dark counts.

We determined the peak fluorescence count for each 397-nm laser power P_{397} and fitted a curve for the signal S as a function of laser power: $S = c/(1 + s/P_{397})$, where

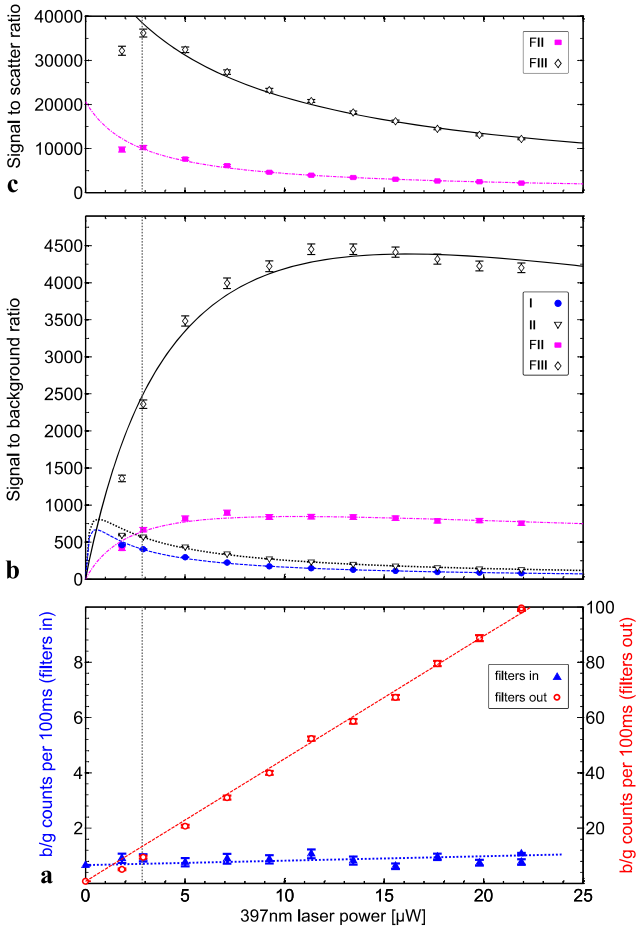

Fig. 5 **a** Background counts versus 397-nm laser power without the filters (*open circles*, *right ordinate*) and with the filters (*filled triangles*, *left ordinate*) including straight-line fits. **b** Signal-to-background ratio versus 397-nm laser power for the four different repumping schemes, with fitted curves. Data points for the lowest 397-nm intensity are shifted down, which may be due to a systematic reduction in the measured peak signal at very low intensities where the resonance becomes narrow and the peak fluorescence could be reduced, e.g. by finite laser line width. **c** Signal-to-scattered light ratio for the two schemes FII and FIII (for the schemes without the filters, this ratio is very similar to the signal-to-background ratio). The *vertical dotted line* shows the 397-nm laser power corresponding to the saturation intensity $I_{\mathrm{sat}} = 2.8\ \mathrm{mW/mm^2}$

s and c are constants. Although strictly appropriate only to a two-level system, we find that this formula is also in good agreement with calculations from our optical Bloch equations model. The four data sets are shown in Fig. 5b as signal-to-background points. The fitted curves, divided by the respective background slopes, are also shown. The standard scheme I has a peak signal-to-background ratio of 670. This is slightly improved by scheme II to 810. Both maxima are narrow peaks and occur at low laser intensity ($\sim 0.2 I_{\mathrm{sat}}$), where the reduced fluorescence leads to a smaller signal-to-noise ratio and a lower cooling efficiency. With the filters in, scheme FII achieves a signal-to-background ratio of 850, which, while only slightly better than the previous results, is maintained over a wide range of 397-nm laser powers and is only gradually reduced in the limit of high laser power. The true merit of our technique can be seen in the results for scheme FIII: the signal-to-background ratio achieved is similar to the standard scheme at low intensities but then rises steeply and peaks at 4400. The peak is again very broad, which makes the method insensitive to the laser intensity. At typical experimental parameters ($P_{397} \approx 10\ \mu\mathrm{W}$) the method surpasses the standard 397 nm + 866 nm scheme I by more than an order of magnitude.

Since, with the filters, the background is dominated by the dark counts, which are highly detector dependent, it is important to consider also the ratio of signal to scattered laser light. This is shown for the two schemes with the filters in Fig. 5c, and has a maximum of 36000 for the scheme FIII. This occurs at a 397-nm laser power corresponding to approximately one saturation intensity ($2.8\ \mathrm{mW/mm^2}$), which offers a good compromise between high scattering rate and low Doppler cooling temperature. For a different detector, such as a cooled EMCCD at the same 100-ms integration time, the dark counts can be negligible and the signal-to-background achievable should be close to this signal-to-scatter ratio.

5 Applications and outlook

Wherever ions are trapped close to surfaces and scattered light from the laser cooling beam is an issue, this technique can be implemented to increase significantly the signal-to-background ratio. This is the case in miniaturized scalable trap geometries for QIP as well as other recent experiments in ion traps. Apart from the cavity and fiber applications mentioned in the introduction, trapped ions are used in sensor applications [28] employing them as field probes in specifically designed traps [29]. Other areas of study are ion–surface interactions and surface plasmon experiments in nano-wires [9]. In all these cases, the ease of implementation with only broadly stabilized diode lasers as well as its ready applicability to other ion species with similar level structures make this scheme attractive.

A low background level is important not only for ion detection, but also for accurate compensation of ion micromotion (for example, by the standard technique of RF/photon arrival time correlation [30]) or for thermometry, as recently described in [31]. Our scheme can also be used in conjunction with heating rate measurements by Doppler recooling, as described in [32]. The theory given in [32] is based on a two-level system, which is not realized exactly in the standard repumping scheme I involving three levels connected in a Λ arrangement. Repumping with the 850-nm and 854-nm lasers (scheme II) gives a close approximation to a two-level system, as discussed in [24], which allows simple interpretation of the Doppler recooling data to extract the heating rate.

In cases where there is high background scatter, scheme FII can be employed.

Acknowledgements We are extremely grateful to Sandia National Laboratories for their fabrication of the trap. The optical Bloch equation simulations were implemented using NAG software. We would also like to acknowledge Alice Burrell for the construction of the imaging system, Graham Quelch for laboratory support and Luca Guidoni for comments on the manuscript. This work was supported by the EPSRC Science and Innovation programme.

References

1. D.J. Wineland, D. Leibfried, Laser Phys. Lett. **8**, 175 (2011)
2. D. Leibfried, R. Blatt, C. Monroe, D. Wineland, Rev. Mod. Phys. **75**, 281 (2003)
3. G. Brady, A. Ellis, D. Moehring, D. Stick, C. Highstrete, K. Fortier, M. Blain, R. Haltli, A. Cruz-Cabrera, R. Briggs, J. Wendt, T. Carter, S. Samora, S. Kemme, Appl. Phys. B **103**, 801 (2011)
4. A. Dantan, J.P. Marler, M. Albert, D. Guénot, M. Drewsen, Phys. Rev. Lett. **105**, 103001 (2010)
5. D.R. Leibrandt, J. Labaziewicz, V. Vuletić, I.L. Chuang, Phys. Rev. Lett. **103**, 103001 (2009)
6. C. Russo, H. Barros, A. Stute, F. Dubin, E. Phillips, T. Monz, T. Northup, C. Becher, T. Salzburger, H. Ritsch, P. Schmidt, R. Blatt, Appl. Phys. B **95**, 205 (2009)
7. M. Keller, B. Lange, K. Hayasaka, W. Lange, H. Walther, J. Mod. Opt. **54**, 1607 (2007)
8. N. Daniilidis, T. Lee, R. Clark, S. Narayanan, H. Häffner, J. Phys. B, At. Mol. Opt. Phys. **42**, 154012 (2009)
9. M. Brownnutt, Pers. Commun. (2011)
10. G. Sagué, E. Vetsch, W. Alt, D. Meschede, A. Rauschenbeutel, Phys. Rev. Lett. **99**, 163602 (2007)
11. E. Vetsch, D. Reitz, G. Sagué, R. Schmidt, S.T. Dawkins, A. Rauschenbeutel, Phys. Rev. Lett. **104**, 203603 (2010)
12. W.K. Hensinger, D.W. Utami, H.-S. Goan, K. Schwab, C. Monroe, G.J. Milburn, Phys. Rev. A **72**, 041405 (2005)
13. S. Chu, L. Hollberg, J.E. Bjorkholm, A. Cable, A. Ashkin, Phys. Rev. Lett. **55**, 48 (1985)
14. J. Eschner, G. Morigi, F. Schmidt-Kaler, R. Blatt, J. Opt. Soc. Am. B **20**, 1003 (2003)
15. A.H. Burrell, D.Phil. thesis, University of Oxford (2010)
16. R.J. Hendricks, J.L. Sørensen, C. Champenois, M. Knoop, M. Drewsen, Phys. Rev. A **77**, 021401 (2008)
17. H. Ohadi, M. Himsworth, A. Xuereb, T. Freegarde, Opt. Express **17**, 23003 (2009)
18. A.H. Myerson, D.J. Szwer, S.C. Webster, D.T.C. Allcock, M.J. Curtis, G. Imreh, J.A. Sherman, D.N. Stacey, A.M. Steane, D.M. Lucas, Phys. Rev. Lett. **100**, 200502 (2008)
19. M.D. Barrett, B. DeMarco, T. Schaetz, V. Meyer, D. Leibfried, J. Britton, J. Chiaverini, W.M. Itano, B. Jelenković, J.D. Jost, C. Langer, T. Rosenband, D.J. Wineland, Phys. Rev. A **68**, 042302 (2003)
20. M. Harlander, M. Brownnutt, W. Hänsel, R. Blatt, New J. Phys. **12**, 093035 (2010)
21. D. Stick, K.M. Fortier, R. Haltli, C. Highstrete, D.L. Moehring, C. Tigges, M.G. Blain. arXiv:1008.0990v2 (2010)
22. D.T.C. Allcock, T.P. Harty, H.A. Janacek, N.M. Linke, C.J. Ballance, D.N. Stacey, A.M. Steane, D.M. Lucas, R.L. Jarecki Jr., S.D. Habermehl, M.G. Blain, D. Stick, D.L. Moehring, Appl. Phys. B (2011, this issue)
23. D.M. Lucas, A. Ramos, J.P. Home, M.J. McDonnell, S. Nakayama, J.-P. Stacey, S.C. Webster, D.N. Stacey, A.M. Steane, Phys. Rev. A **69**, 012711 (2004)
24. D.T.C. Allcock, J.A. Sherman, D.N. Stacey, A.H. Burrell, M.J. Curtis, G. Imreh, N.M. Linke, D.J. Szwer, S.C. Webster, A.M. Steane, D.M. Lucas, New J. Phys. **12**, 053026 (2010)
25. R. Gerritsma, G. Kirchmair, F. Zähringer, J. Benhelm, R. Blatt, C.F. Roos, Eur. Phys. J. D **50**, 13 (2008)
26. I. Siemers, M. Schubert, R. Blatt, W. Neuhauser, P.E. Toschek, Europhys. Lett. **18**, 139 (1992)
27. G. Shu, N. Kurz, M.R. Dietrich, B.B. Blinov, Phys. Rev. A **81**, 042321 (2010)
28. G.R. Guthöhrlein, M. Keller, K. Hayasaka, W. Lange, H. Walther, Nature **414**, 49 (2001)
29. R. Maiwald, D. Leibfried, J. Britton, J.C. Bergquist, G. Leuchs, D.J. Wineland, Nat. Phys. **5**, 551 (2009)
30. D.J. Berkeland, J.D. Miller, J.C. Bergquist, W.M. Itano, D.J. Wineland, J. Appl. Phys. **83**, 5025 (1998)
31. E.W. Streed, M.J. Petrasiunas, A. Jechow, D. Kielpinski, B.G. Norton, New. J. Phys. **13**, 113022 (2011)
32. J.H. Wesenberg, R.J. Epstein, D. Leibfried, R.B. Blakestad, J. Britton, J.P. Home, W.M. Itano, J.D. Jost, E. Knill, C. Langer, R. Ozeri, S. Seidelin, D.J. Wineland, Phys. Rev. A **76**, 053416 (2007)